

Electrical detection of T_{V2a} -type silicon vacancy spin defect in 4H-SiC MOSFETs

Cite as: Appl. Phys. Lett. **120**, 064001 (2022); <https://doi.org/10.1063/5.0078189>

Submitted: 11 November 2021 • Accepted: 11 January 2022 • Published Online: 08 February 2022

 Yuta Abe, Akihumi Chaen,  Mitsuru Sometani, et al.



View Online



Export Citation



CrossMark

ARTICLES YOU MAY BE INTERESTED IN

[Special topic on materials and devices for 5G electronics](#)

Applied Physics Letters **120**, 060402 (2022); <https://doi.org/10.1063/5.0079175>

[Thermometric quantum sensor using excited state of silicon vacancy centers in 4H-SiC devices](#)

Applied Physics Letters **118**, 044001 (2021); <https://doi.org/10.1063/5.0027603>

[Characterization methods for defects and devices in silicon carbide](#)

Journal of Applied Physics **131**, 140903 (2022); <https://doi.org/10.1063/5.0077299>



APL Quantum

CALL FOR APPLICANTS

Seeking Editor-in-Chief

Electrical detection of T_{V2a} -type silicon vacancy spin defect in 4H-SiC MOSFETs

Cite as: Appl. Phys. Lett. **120**, 064001 (2022); doi: [10.1063/5.0078189](https://doi.org/10.1063/5.0078189)

Submitted: 11 November 2021 · Accepted: 11 January 2022 ·

Published Online: 8 February 2022



View Online



Export Citation



CrossMark

Yuta Abe,^{1,2} Akihumi Chaen,¹ Mitsuru Sometani,³ Shinsuke Harada,³ Yuichi Yamazaki,² Takeshi Ohshima,^{1,2} and Takahide Umeda^{1,a)}

AFFILIATIONS

¹Institute of Applied Physics, University of Tsukuba, Tsukuba 305-8573, Japan

²National Institutes for Quantum Science and Technology (QST), Takasaki 370-1292, Japan

³National Institute of Advanced Industrial Science and Technology (AIST), Tsukuba 305-8569, Japan

^{a)} Author to whom correspondence should be addressed: umeda.takahide.fm@u.tsukuba.ac.jp

ABSTRACT

Color centers in silicon carbide (4H-SiC) are potentially usable as spin defects for quantum sensing and quantum information technology. In particular, neutral divacancies (the $P6/P7$ centers, $V_{Si}V_C^0$) and a certain type of silicon vacancies (the T_{V2a} center, V_{Si}^- at the k site) are promising for addressing and manipulating single spins. Although the T_{V2a} spin is readable at room temperature, the readout techniques have been limited to luminescence-based ones (e.g., optically detected magnetic resonance). In this study, we demonstrated electrical detection of T_{V2a} -type silicon vacancies at room temperature by using electrically detected magnetic resonance on 4H-SiC metal–oxide–semiconductor field effect transistors (MOSFETs). T_{V2a} spin defects were embedded in the channel region of well-defined 4H-SiC MOSFETs via controlled proton irradiation. The number of detected T_{V2a} spins was estimated to be $\sim 10^5$. We also found that the charge state of the T_{V2a} spin defect can be controlled by varying the gate voltage applied to the MOSFET.

Published under an exclusive license by AIP Publishing. <https://doi.org/10.1063/5.0078189>

Color centers in wide-bandgap semiconductors are potentially usable as spin defects or spin qubits for quantum sensing,¹ quantum communication,² and quantum computing.³ The negatively charged nitrogen-vacancy center (the NV^- center, electron spin $S = 1$) in diamond is the most widely studied spin qubit, because it shows not only extremely strong luminescence but also its spin states that can be manipulated and readout at room temperature.⁴ Another promising host platform for spin defects is silicon carbide (4H-SiC).⁵ 4H-SiC shows great potential for integration of various electronic devices [pn diodes, bipolar transistors, junction- and metal–oxide–semiconductor field effect transistors (JFETs and MOSFETs) and complementary-MOS (CMOS) circuits].⁶ In particular, 4H-SiC is regarded as a suitable integration platform for electronic and quantum devices. So far, single-spin addressing and single-spin manipulation have been already demonstrated using spin defects in 4H-SiC.^{7–10} 4H-SiC has two promising spin defects: a negatively charged silicon vacancy formed at the k site (the T_{V2a} center, k -site V_{Si}^- , $S = 3/2$)^{7,8} and neutral divacancies (the $P6/P7$ centers, $V_{Si}V_C^0$, $S = 1$).^{9,10} The V_{Si}^- center is the most widely studied, because its optically detected magnetic resonance (ODMR) is detectable at room temperature.^{7,8} Furthermore, creation of V_{Si}^- by versatile means such as proton beam writing¹¹ makes it

possible to design hybrid electronic and quantum devices. However, the V_{Si}^- center has a much weaker ODMR contrast than that of NV^- . To develop other readout techniques as well as all-electrical quantum devices, electrical detection of the V_{Si}^- spin is desirable. Actually, electrical detection of NV^- centers in diamond has recently been demonstrated.¹² In 4H-SiC, electrically detected magnetic resonance (EDMR) was used to detect the V_{Si}^- signal in the device currents of 4H-SiC pn diodes¹³ and 4H-SiC MOSFETs.¹⁴ In MOSFETs, V_{Si}^- centers were generated as MOS interfacial defects,¹⁴ while in pn diodes, they were intentionally created by irradiation.¹³ In the latter case, a strong electrical signal was observed and utilized for high-sensitivity magnetic sensing.¹⁴ Namely, the V_{Si}^- spin is most probably highly active to electrical currents. However, the detected V_{Si}^- center is not the T_{V2a} center [$V_{Si}^-(k)$], which is realized the single spin manipulation at room temperature, but rather only another V_{Si}^- center [negatively charged silicon vacancy formed at the h site, $V_{Si}^-(h)$]. So far, the T_{V2a} -type spin defect has not been detected electrically.

In this Letter, we demonstrate electrical detection of the T_{V2a} spin defect by using the EDMR technique on a proton-irradiated 4H-SiC(0001) MOSFET. The T_{V2a} centers were carefully created in the channel region of the MOSFET via proton irradiation. The 4H-SiC

MOSFETs could generate a high channel current as well as had few EDMR signals from MOS interface defects. These features led to their having higher sensitivity to the spin defect and less interference from interface signals. In a previous EDMR study, we characterized the interface defects in the relevant MOSFET and determined their spin density.¹⁵ By using a coexisting EDMR signal from the interface defects, we could estimate the number of electrically detected $T_{V_{2a}}$ spins.

In addition, by taking advantage of the MOSFET, we could electrically control the charge state for the $T_{V_{2a}}$ spin defect. Here, it is

indispensable to tune its charge state properly for detecting its electron spin. For example, the loss of an electron from the NV^- center in diamond causes severe degradation in luminescence and the ODMR signal.¹⁶ In the present study, we used the gate bias of the MOSFET to tune the charge state of V_{Si} .

Figure 1(a) shows the setup for electrical detection of V_{Si}^- centers in a 4H-SiC MOSFET. In the experiment, we used n -channel lateral Si-face 4H-SiC MOSFETs¹⁵ that include V_{Si} centers in the vicinity of the MOS interface. This setup is based on bipolar-amplification-effect (BAE) EDMR spectroscopy, which is highly and selectively sensitive to

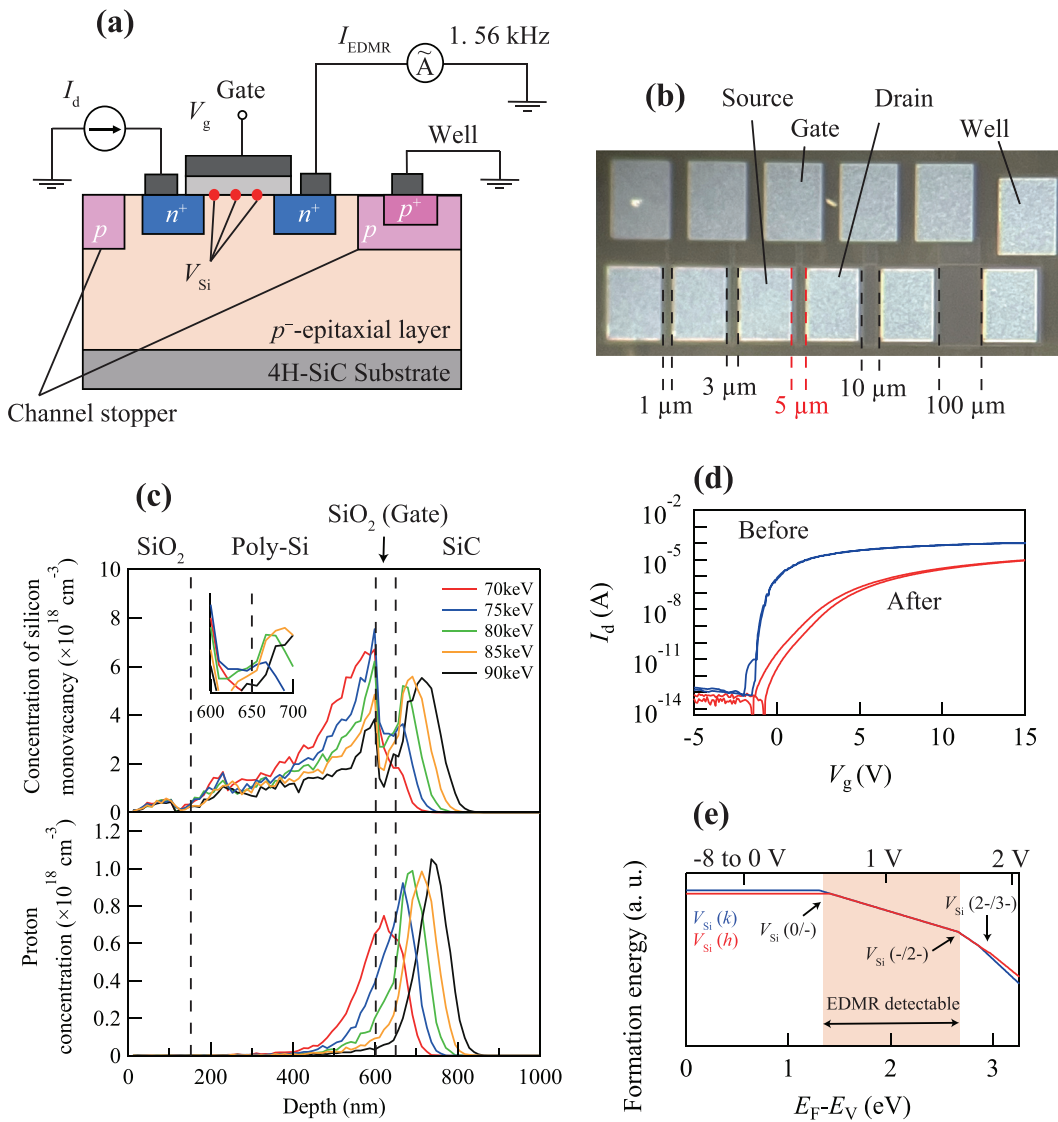


FIG. 1. (a) Electrical detection of V_{Si}^- spin defects embedded in 4H-SiC MOSFETs. We used BAE-EDMR detection. (b) Optical image of 4H-SiC MOSFETs used in the EDMR study. The MOSFET had 5- μm gate length and 150- μm gate width. (c) Simulated depth profiles of implanted protons (lower figure) and silicon-atom monovacancies (upper figure). Depth "0" is defined at the surface of the top passivation SiO_2 layer. TRIM simulations were for a fluence of $1 \times 10^{13} H^+/cm^2$. (d) I_d - V_g characteristic of 4H-SiC MOSFETs before and after proton irradiation. Voltage was swept from -5 to 15 V and back again. (e) Schematic diagram of the formation energy of V_{Si} in 4H-SiC. The charge state of V_{Si} is determined by the Fermi level (E_F) position from the valence band edge (E_V). The Fermi level can be controlled by the gate voltage (V_g) of MOSFETs, and top of diagram shows V_g applied during EDMR measurement. The region highlighted in orange is the range of the Fermi level that V_{Si}^- is detectable by EDMR.

interface defects.^{17,18} The MOSFETs used in this study had a gate length of $5\ \mu\text{m}$ [Fig. 1(b)], which is the best for BAE-EDMR measurements. The MOSFETs have 50-nm-thick gate thermal oxide and were subjected to standard post oxidation annealing in NO gas at $1250\ ^\circ\text{C}$ for 60 min, which improved their field-effect mobility to $30\ \text{cm}^2\text{V}^{-1}\text{s}^{-1}$. The EDMR signal from the interface defects was dramatically reduced by $1/40$.¹⁵

To create V_{Si} defects inside the channel region, we carried out proton irradiation with a fluence of $1 \times 10^{13}\ \text{cm}^{-2}$ over the whole of the MOSFET. It is known that proton irradiation can create V_{Si} defects around the ion-stop region in SiC crystals.¹⁹ Figure 1(c) shows simulated depth profiles of protons and silicon-atom monovacancies in a gate-stack structure, which were obtained by the Monte Carlo simulation code, TRIM.²⁰ The top SiO_2 layer is a protective passivation layer (150 nm). The acceleration energy can be used to control the formation of V_{Si} defects precisely. We chose 80 keV, at which a sharp distribution (peak width $\sim 30\ \text{nm}$) of Si monovacancies may be obtained, as shown in Fig. 1(c). This distribution fully covers the thickness of the channel layer (7–8 nm) of the present MOSFET.

Before irradiation, the MOSFETs were characterized using EDMR¹⁵ and various other techniques.²¹ Their drain current (I_d)-gate voltage (V_g) characteristics are shown in Fig. 1(d). The drain current after irradiation decreased compared with the value before irradiation, as a result of implantation damage. The field-effect mobility fell to $10\ \text{cm}^2\text{V}^{-1}\text{s}^{-1}$, and hysteresis increased slightly. Despite that the proton irradiation degraded the electrical characteristics the MOSFET in these ways, it was still usable for the BAE-EDMR measurements reported below. The charge state of V_{Si} is determined by the Fermi level [Fig. 1(e)]. The range of the Fermi level that the charge state of V_{Si} is singly negative is 1.3–2.66 eV from the valence band edge.²² In order to detect V_{Si} by EDMR, the gate voltage of the MOSFET must be applied so that the Fermi level is within this range. We discuss this later in Fig. 3.

BAE-EDMR measurements were carried out at room temperature under microwave excitation (9.462 GHz and 200 mW) and magnetic-field modulation at 1.562 kHz and 0.5-mT width. We introduced constant current (I_d) from the drain electrode and monitored the source current (I_{EDMR}). Using a lock-in amplifier synchronized with the magnetic-field modulation, electron-spin-resonance (ESR)-induced current changes in I_{EDMR} were recorded as a function of the static magnetic field. The magnetic field was rotated in the (1 $\bar{1}$ 00) plane. Figure 2(a) shows the angular dependence of the EDMR spectra for the MOSFETs before and after irradiation. The blue spectra obtained before irradiation reveal higher signal intensities; their intensities are, thus, normalized to those of the red spectra obtained after irradiation. In other words, proton irradiation degraded the EDMR detection. This may have been caused by the drain-current degradation [cf. Fig. 1(d)], although the exact reason is still unclear. A strong central signal [indicated by the black arrow in Fig. 2(a)] was detected from both the irradiated MOSFET and non-irradiated one: it originates from nitrogen-related interface defects of nitrided 4H-SiC(0001) MOS interfaces.¹⁵ After irradiation, a new doublet signal with zero-field splitting appeared (the red arrows in the figure). Figure 2(b) plots the position of the new signal as a function of the magnetic-field angle. The observed angular dependence is consistent with that of the $T_{V_{2a}}$ spin defect that was calculated from the spin-Hamiltonian of $T_{V_{2a}}$ (g value, $g = 2.0029$, and fine-splitting parameters, $D = 35\ \text{MHz}$, $E = 0$).²³

This result indicates we demonstrated to detect the $T_{V_{2a}}$ spin defect [the $V_{\text{Si}}^-(k)$ center] electrically.

To discuss the central spectral region where another type of V_{Si}^- [the $V_{\text{Si}}^-(h)$ center] exhibits a single-peak signal without zero-field splitting, we performed an analysis by subtracting the EDMR spectrum before irradiation from that after irradiation. Figure 2(c) shows two typical results where the $V_{\text{Si}}^-(k)$ and $V_{\text{Si}}^-(h)$ signals either overlap or do not overlap. A single-peak signal seems to appear near the interface signal. Moreover, this signal seems to be isotropic [cf. Fig. 2(b)] and is consistent with the $V_{\text{Si}}^-(h)$ signal. However, its position does not exactly match the theoretical positions of $V_{\text{Si}}^-(h)$. We deduce that this inconsistency may be due to distortion from the interface EDMR signal. This signal consists of two components: a signal from the interfacial K center ($\text{Si}\equiv\text{N}_3$) and one from the incomplete K center ($\text{Si}\equiv\text{C}_2\text{N}$).¹⁵ Therefore, the proton irradiation may have modified these interface defects by knocking out nitrogen atom(s). As a result, the interface EDMR signal may have become distorted after irradiation, resulting in a constant shift of the subtracted signal.

Here, let us estimate the number of detected $T_{V_{2a}}$ spins by referring to the coexisting interface signal. It was reported that the interface signal corresponds to a spin density of $2.6 \times 10^{11}\ \text{cm}^{-2}$ (the total density of K centers and incomplete K centers estimated for the “NO60” specimen).¹⁵ Since the gate area of the present MOSFET is $1 \times 10^{-5}\ \text{cm}^2$ ($200 \times 5\ \mu\text{m}^2$), the number of interface “spins” is estimated to be 2.6×10^6 . We assume that the area of the integrated EDMR signal (absorption EDMR signal) is proportional to the number of detected spins. Comparing the area of the $T_{V_{2a}}$ signal with that of the interface signal, we deduce the number of observed $T_{V_{2a}}$ centers to be 1×10^5 spins for our experimental setup.

Next, we measured the EDMR spectra for various gate voltages and plotted the signal intensities of $T_{V_{2a}}$ (peak-to-peak signal heights) and the relevant detection currents (I_{EDMR}) as a function of V_g [Fig. 3(a)]. The $T_{V_{2a}}$ signal was only detectable at around $V_g = 0\ \text{V}$ (-2 to $+1\ \text{V}$), implying that the V_{Si} center was singly negatively charged in this V_g range. In other words, its charge state changed from -1 to -2 above $V_g = 2\ \text{V}$ and from -1 to zero below $V_g = -3\ \text{V}$. To examine the gate-bias dependence of the charge states of V_{Si} , we carried out capacitance-voltage (C - V) measurements and determined the Fermi level (E_F) for each V_g . For this purpose, we used a p -type MOS capacitor that imitated the gate-stack structure of the present n -channel MOSFET. The MOS capacitor and the MOSFETs were from the same test-element-group SiC chip, meaning that they had been subjected to the same fabrication process as well as the same irradiation. Figure 3(b) shows the C - V curves of the MOS capacitor, where V_g was swept from -20 to $20\ \text{V}$ and then back again. In the figure, the constant-capacitance region in the downward sweep is caused by the pinning effect due to interface defects. Using the above $C(V_g)$ data, we estimated E_F at the MOS interface by using equation (1) of Ref. 24. In Fig. 3(b), the calculated E_F values are shown with respect to the valence band top (E_V). As noted earlier, the E_F pinning occurred in the range between -10 and $0\ \text{V}$. Above $0\ \text{V}$, E_F rose rapidly toward the conduction band bottom (E_C). This behavior matched that of the detected current in Fig. 3(a), which rapidly increased through the formation of the inversion layer.

Figure 3(c) draws the E_F position for each V_g together with the theoretical ($0/-$), ($-2/-$) and ($2-/3-$) levels of $V_{\text{Si}}(k)$ and $V_{\text{Si}}(h)$.^{22,25} The V_{Si} centers can change their charge states from 0 to -3 depending

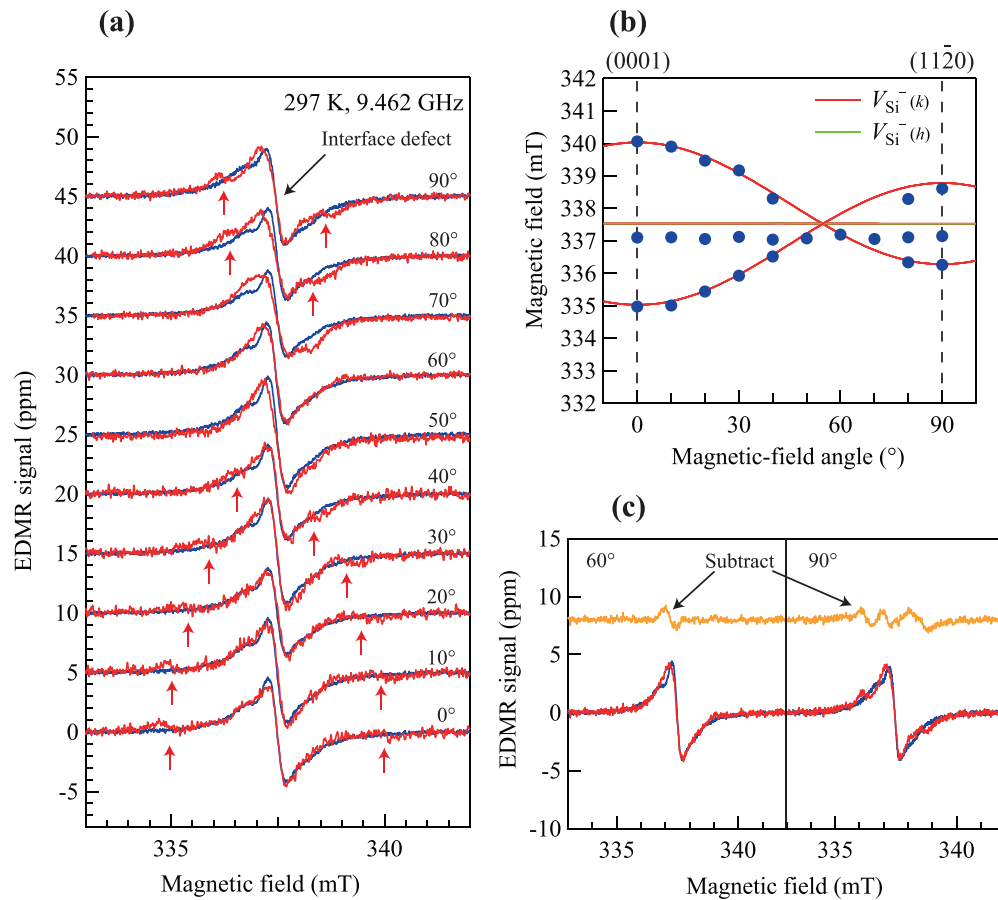


FIG. 2. (a) EDMR spectra of proton irradiated 4H-SiC MOSFETs measured at room temperature and with different magnetic fields. Each spectrum after irradiation (red line) was measured under $I_{\text{EDMR}} = 600$ nA and $V_g = 0$ V. Spectra before irradiation (blue lines) were measured under $I_{\text{EDMR}} = 500$ nA and $V_g = -5$ V. The blue spectra obtained before irradiation reveal higher signal intensities; their intensities are, thus, *normalized* to those of the red spectra obtained after irradiation. The black arrow indicates the EDMR signal from the interface defects.¹⁵ Red arrows correspond to a spin defect of $V_{\text{Si}}^-(k)$ (T_{V2a} center) with a zero-field splitting of 70 MHz. (b) Angular map of EDMR signals. Solid lines are theoretical values calculated for $V_{\text{Si}}^-(k)$ (T_{V2a} , $S = 3/2$) and $V_{\text{Si}}^-(h)$ ($S = 3/2$, without zero-field splitting). (c) Difference between EDMR spectra before and after irradiation, showing the possible presence of a single-peak signal [probably due to $V_{\text{Si}}^-(h)$] close to the interface signal.

on E_F . Looking at this diagram, the T_{V2a} spin defect is only detectable at $V_g = 1$ V, which is consistent with the experimental result. However, it is likely that the T_{V2a} signal was still observable under some negative V_g biases, where V_{Si}^0 should be stable, an apparent discrepancy. We suggest that the reason for this discrepancy may be the distribution of V_{Si}^- defects, which formed not only at the MOS interface but also at deeper positions. EDMR measures the whole of V_{Si}^- in the channel layer. On the contrary, the above E_F estimation is valid just at the MOS interface. Accordingly, the EDMR result is affected by deeper V_{Si}^- defects that feel a weaker V_g dependence as compared to those at the interface. As a result, we can expect there to be a mismatch of the gate-bias dependences.

Although electrical detection of the T_{V2a} spin defect was demonstrated, its sensitivity was extremely low. For instance, the accumulation time for recording an EDMR spectrum such as the one shown in Fig. 2 was as long as 12 hours. However, we should note that another type of V_{Si}^- spin [$V_{\text{Si}}^-(h)$] was used to make an electric-circuit-based magnetic sensor with ultra-high sensitivity,¹³ implying that the T_{V2a}

spin [$V_{\text{Si}}^-(k)$] also acts as a highly electrically-active color center, and this would enable us to electrically access its spin state with high sensitivity. Thus, in principle, it should be possible for the sensitivity to be dramatically improved by making a number of optimizations. The first would be to further increase the detection current. As mentioned above, proton irradiation substantially degraded the detection current as well as the EDMR signals. By optimizing the formation process of V_{Si}^- , the EDMR sensitivity could be dramatically increased. For instance, the proton beam writing (PBW) technique is useful to create V_{Si}^- selectively.¹¹ Proton irradiation in this study degraded the MOSFETs since irradiation was performed on whole of the MOSFETs. PBW can create V_{Si}^- with fewer degradation of the MOSFETs than this study. After irradiation, some amounts of residual defects can be removed by relatively-low temperature annealing without V_{Si}^- disassociation.²⁶ In addition, the device design could be optimized: e.g., a comb-shaped gate pattern would vastly increase the channel current (i.e., the detection current). Other improvements can be made by lowering the detection temperature and by illuminating

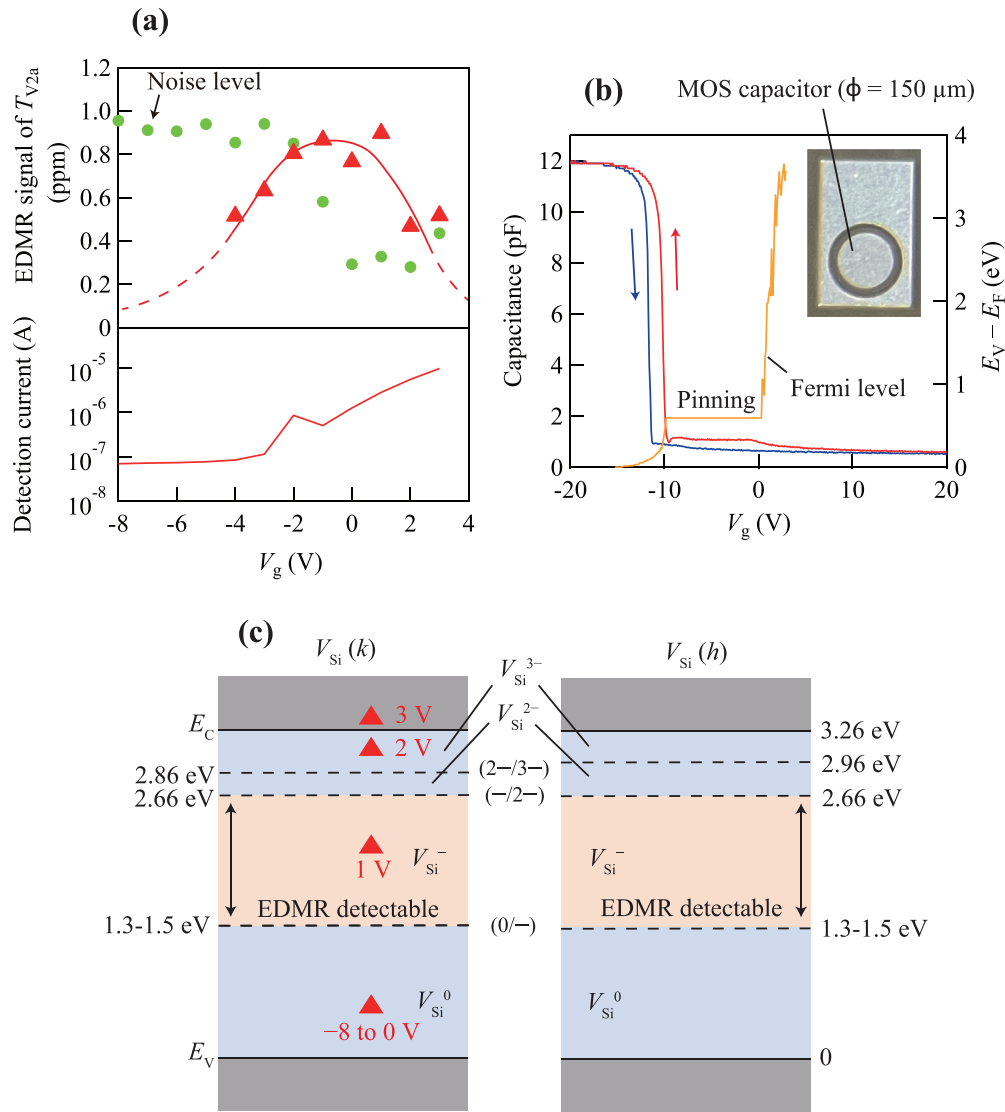


FIG. 3. (a) Gate-bias (V_g) dependence of the EDMR signal intensity of T_{V2a} spin defects and detection current (I_{EDMR}) for EDMR. The T_{V2a} spin defect was clearly observed within a limited V_g range (-2 to 1 V). Noise levels of EDMR detection are also shown. (b) Estimation of the Fermi level (E_F) vs V_g from MOS C-V measurements. The left axis indicates C-V curves measured for the p-MOS capacitor, from which we calculated E_F at the MOS interface shown in the right axis. (c) Energy-band diagram of 4H-SiC and charge states of the V_{Si} center determined by first-principles calculation.^{22,25} The region highlighted in orange is the ideal detectable range for the V_{Si}^{-} spin defect. Red triangles indicate E_F positions vs V_g determined from (b).

the light (by causing photo-induced spin polarization), which both enhance the populational difference between the spin levels as well as the resultant ESR signal. In fact, the ESR signal of T_{V2a} was strongly enhanced under such conditions.²⁷ Combining these methods will make it possible for quantum technologies to detect the T_{V2a} spin defect electrically.

In summary, we introduced V_{Si} spin defects [the T_{V2a} center or $V_{Si}^{-}(k)$, $S = 3/2$, zero-field splitting = 70 MHz] into the channel region of 4H-SiC MOSFETs by using optimized proton irradiation. By taking advantage of the BAE-EDMR technique, which is highly sensitive to interface defects, we demonstrated electrical detection of the T_{V2a}

EDMR signal at room temperature. This center had already been established to be an optically detectable spin qubit, and our experiment shows that it is also electrically detectable. We also showed that the charge state of the T_{V2a} spin defect could be controlled by varying the gate bias of the MOSFET. Furthermore, this MOSFET platform enabled us to estimate the number of detected T_{V2a} spins, because its MOS interface provides a reference EDMR signal whose spin density is known. The number of electrically detected T_{V2a} spins was roughly estimated to be 1×10^5 . At the present stage, the sensitivity of electrical detection is extremely low. However, much higher sensitivity is believed to be possible, and we discussed various ways of improving it.

This work was partly supported by JSPS KAKENHI via Grant Nos. 20H00340, 20H00355, and 21H04553.

AUTHOR DECLARATIONS

Conflict of Interest

The authors declare no conflict of interest.

DATA AVAILABILITY

The data that support the findings of this study are available from the corresponding author upon reasonable request.

REFERENCES

- ¹L. Rondin, J.-P. Tetienne, T. Hingant, J.-F. Roch, P. Maletinsky, and V. Jacques, *Rep. Prog. Phys.* **77**, 056503 (2014).
- ²E. Togan, Y. Chu, A. S. Trifonov, L. Jiang, J. Maze, L. Childress, M. V. G. Dutt, A. S. Sørensen, P. R. Hemmer, A. S. Zibrov, and M. D. Lukin, *Nature* **466**, 730 (2010).
- ³M. D. Reed, L. DiCarlo, S. E. Nigg, L. Sun, L. Frunzio, S. M. Girvin, and R. J. Schoelkopf, *Nature* **482**, 382 (2012).
- ⁴P. Neumann, J. Beck, M. Steiner, F. Rempp, H. Fedder, P. R. Hemmer, J. Wrachtrup, and F. Jelezko, *Science* **329**, 542 (2010).
- ⁵S. Castelletto and B. Alberto, *J. Phys.: Photonics* **2**, 022001 (2020).
- ⁶T. Kimoto, *Jpn. J. Appl. Phys., Part 1* **54**, 040103 (2015).
- ⁷M. Widmann, S.-Y. Lee, T. Rendler, N. Tien Son, H. Fedder, S. Pirk, L.-P. Yang, N. Zhao, S. Yang, I. Booker, A. Denisenko, M. Jamali, S. A. Momenzadeh, I. Gerhardt, T. Ohshima, A. Gali, E. Janzén, and J. Wrachtrup, *Nat. Mater.* **14**, 164 (2015).
- ⁸M. Widmann, M. Niethammer, D. Y. Fedyanin, I. A. Khramtsov, T. Rendler, I. D. Booker, J. Ul Hassan, N. Morioka, Y. C. Chen, I. G. Ivanov, N. T. Son, T. Ohshima, M. Bockstedte, A. Gali, C. Bonato, S. Y. Lee, and J. Wrachtrup, *Nano Lett.* **19**(10), 7173 (2019).
- ⁹D. J. Christle, A. L. Falk, P. Andrich, P. V. Klimov, J. Ul Hassan, N. T. Son, E. Janzén, T. Ohshima, and D. D. Awschalom, *Nat. Mater.* **14**, 160 (2015).
- ¹⁰C. F. de las Casas, D. J. Christle, J. Ul Hassan, T. Ohshima, N. T. Son, and D. D. Awschalom, *Appl. Phys. Lett.* **111**, 262403 (2017).
- ¹¹Y. Yamazaki, Y. Chiba, T. Makino, S. I. Sato, N. Yamada, T. Satoh, Y. Hijikata, K. Kojima, S. Y. Lee, and T. Ohshima, *J. Mater. Res.* **33**(20), 3355 (2018).
- ¹²E. Bourgeois, E. Londero, K. Buczak, J. Hruby, M. Gulka, Y. Balasubramaniam, G. Wächter, J. Stursa, K. Dobes, F. Aumayr, M. Trupke, A. Gali, and M. Nesladek, *Phys. Rev. B* **95**, 041402 (2017).
- ¹³C. J. Cochrane, J. Blacksberg, M. A. Anders, and P. M. Lenahan, *Sci. Rep.* **6**, 37077 (2016).
- ¹⁴C. J. Cochrane, P. M. Lenahan, and A. J. Lelis, *J. Appl. Phys.* **109**, 014506 (2011).
- ¹⁵E. Higa, M. Sometani, H. Hirai, H. Yano, S. Harada, and T. Umeda, *Appl. Phys. Lett.* **116**, 171602 (2020).
- ¹⁶M. V. Hauf, B. Grotz, B. Naydenov, M. Dankerl, S. Pezzagna, J. Meijer, F. Jelezko, J. Wrachtrup, M. Stutzmann, F. Reinhard, and J. A. Garrido, *Phys. Rev. B* **83**, 081304 (2011).
- ¹⁷T. Aichinger and P. M. Lenahan, *Appl. Phys. Lett.* **101**, 083504 (2012).
- ¹⁸M. A. Anders, P. M. Lenahan, C. J. Cochrane, and A. J. Lelis, *IEEE Trans. Electron Devices* **62**, 301 (2015).
- ¹⁹H. Kraus, D. Simin, C. Kasper, Y. Suda, S. Kawabata, W. Kada, T. Honda, Y. Hijikata, T. Ohshima, V. Dyakonov, and G. V. Astakhov, *Nano Lett.* **17**, 2865 (2017).
- ²⁰J. F. Ziegler, M. D. Ziegler, and J. P. Biersack, *Nucl. Instrum. Methods B* **268**(11–12), 1818 (2010).
- ²¹T. Hatakeyama, Y. Kiuchi, M. Sometani, S. Harada, D. Okamoto, H. Yano, Y. Yonezawa, and H. Okumura, *Appl. Phys. Express* **10**, 046601 (2017).
- ²²M. E. Bathen, A. Galeckas, J. Müting, H. M. Ayedh, U. Grossner, J. Coutinho, Y. K. Frodason, and L. Vines, *npj Quantum Inf.* **5**, 1 (2019).
- ²³N. Mizuochi, S. Yamasaki, H. Takizawa, N. Morishita, T. Ohshima, H. Itoh, and J. Isoya, *Phys. Rev. B* **66**, 235202 (2002).
- ²⁴E. H. Poindexter, G. J. Gerardi, M.-E. Rueckel, P. J. Caplan, N. M. Johnson, and D. K. Biegelsen, *J. Appl. Phys.* **56**, 2844 (1984).
- ²⁵T. Hornos, A. Gali, and B. G. Svensson, *Mater. Sci. Forum* **679–680**, 261 (2011).
- ²⁶Y. Chiba, Y. Yamazaki, S. Sato, T. Makino, N. Yamada, T. Sato, Y. Hijikata, and T. Ohshima, *Mater. Sci. Forum* **1004**, 337 (2020).
- ²⁷J. Isoya, T. Umeda, N. Mizuochi, and T. Ohshima, *Mater. Sci. Forum* **615–617**, 353 (2009).